

Synthesizing and Optimizing Rutile TiO₂ Nanoparticles for Magnetically Guided Drug Delivery

Shilpy Bhullar¹, Navdeep Goyal¹, Shikha Gupta ²

¹Department of Physics, Centre of Advanced Study in Physics, Panjab University, Chandigarh, 160014, India; ²Department of Physics, Goswami Ganesh Dutta Sanatan Dharma College, Chandigarh, 160032, India

Correspondence: Shikha Gupta, Department of Physics, Goswami Ganesh Dutta Sanatan Dharma College, Sector-32c, Chandigarh, 160032, India, Email shikhagupta16@gmail.com

Introduction: Titanium dioxide nanoparticles (TiO₂ NPs) have shown tremendous potential in targeted drug-delivery applications. Among various mechanisms, magnetically guided transport of drugs is one such technique for the said purpose. TiO₂ NPs being diamagnetic or sometimes exhibiting very weak ferromagnetism can be modified by treating them with suitable magnetic materials.

Methods: Rutile TiO₂ NPs were synthesized and doped with Iron Supplement FericipXT and rare-earth metals like cerium, erbium and neodymium via sol-gel technique. FericipXT-coated rutile TiO₂ NPs were synthesized in three different core-shell ratios (1:3, 1:1 and 3:1). The resulting samples were characterized via X-ray Diffraction (XRD), Vibrating Sample Magnetometer (VSM) and High-Resolution Transmission Electron Microscopy (HR-TEM).

Results: XRD of FericipXT-doped TiO₂ NPs showed a rutile phase for 1% and 3% doping; however, only a small fraction of the maghemite phase was obtained for 5% doping. The XRD plots of Ce-doped, Er-doped and Nd-doped TiO₂ NPs showed a variety of phases of TiO₂ NPs (such as anatase/rutile/mixed) along with the oxide phases of the corresponding rare-earth metal. The presence of various iron titanium oxides and iron oxides was found in core-shell NPs. HR-TEM images confirmed the formation of 1:3, 1:1 and 3:1 core-shell TiO₂ NPs. VSM studies showed that the resulting NPs depicted magnetism in the form of superparamagnetism, ferromagnetism and even paramagnetism.

Discussion: The doping to 3% does not affect the original phase of the resulting TiO₂ NPs as depicted from the XRD; however, a doping of 5% and more resulted in extra phases corresponding to the dopant added. FericipXT was loaded over TiO₂ NPs in amorphous form. Among all the samples synthesized, FericipXT-coated TiO₂ NPs demonstrated the best magnetic ability. It was deduced that coating with a magnetic material drastically improves the magnetic character of the host NPs.

Keywords: magnetically-guided drug delivery, drug delivery, rare-earth metals, iron supplement, TiO₂ nanoparticles, superparamagnetism, paramagnetism, ferromagnetism

Introduction

Today, various nanomaterials are being studied, processed and modified for optimizing their bioactivity and therapeutic effects. These nanomaterials include metal nanoparticles (NPs), metal oxide NPs, nano-bioceramics, dendrimers, polymeric NPs, micelles, exosomes, liposomes, ferrites, quantum dots, nanocomposites and many more. An emphasis is laid on applying an economical route for the synthesis of nanomaterials. To avail maximum advantages, an amalgamation of different materials is fabricated to reap the benefits of all the individual materials. For instance, Bagheri et al¹ reinforced epoxy hybrid/glass fibres with nanoclay to form a composite and found an improvement in the tensile strength. On similar grounds, scientists are preferring metal oxide NPs over metal NPs as these technological materials have more features to offer. Among various categories of nanomaterials, magnetic NPs are gaining a lot of attention due to their ease of synthesis, ability to respond to applied magnetic fields and utility in multiple applications. The magnetically-responsive nanomaterials have a plethora of applications such as targeted drug delivery, hyperthermia treatment, water

filtration, sensors and many other applications. Takmil et al² prepared activated charcoal/Fe₃O₄ nanocomposite for wastewater treatment. Mousavi et al³ decorated graphene oxide with Fe₃O₄ NPs for the adsorption of erythrosine from an aqueous solution. In another study, graphene oxide/Fe₃O₄ NPs were studied for their ability to remove lead from wastewater.⁴ Parvin et al⁵ synthesized magnetic nano-adsorbents by decorating graphene oxide with Fe₃O₄ for the removal of phenolic compounds. Hashemi et al⁶ synthesized polyaniline-Fe₃O₄-silver diethyldithiocarbamate nanocomposite for detecting mercury in non-biological or biological aqueous media at the picomolar level. In the regime of biomedical applications, magnetic NPs are highly recommended for novel cancer therapies because of their maximal benefits and fewer side-effects on the human body. The NPs exhibiting superparamagnetism are utilized in Magnetic Resonance Imaging (MRI). Magnetic NPs can ensure targeted delivery of the drug when guided through an applied magnetic field. These NPs, when heated, can trigger release of the drug trapped and in some cases, can also result in hyperthermia in carcinogenic tissues.⁷ Soltani et al⁸ reported that magnetic NPs can effectively kill the malignant cells via microwave ablation. They also stated that smaller sized NPs increase the percent area of ablation due to their enhanced diffusion into the tumor. Salmani et al⁹ reported the soft magnetic property of zirconium-ferrite (Zr-Fe₃O₄) treated bioceramics which indicated the significant potential of the synthesized composite in biomedical applications. Mousavi et al¹⁰ synthesized polyrhodanine/Fe₃O₄ modified with graphene oxide which demonstrated effective antibacterial and anticancer properties. Rezaeian et al¹¹ devised a mathematical model to study the efficacy of magnetically-controlled targeted delivery of drugs using magnetic NPs in intraperitoneal chemotherapy as compared to the drug delivery in conventional intraperitoneal chemotherapy. The results showed an increase in the drug penetration depth, drug penetration area, cancer cell apoptosis and overall efficiency of the magnetically-guided chemotherapy as compared to conventional chemotherapy. All these works involve the use of magnetic Fe₃O₄ as the application part is based on applying a magnetic field to attain the desired response. A number of in-vitro and in-vivo studies are performed to ascertain the efficacy of the drug-loaded nanomaterials under particular physiological conditions. Different simulated fluids are prepared to mimic the bodily fluids to test the behaviour of NPs for specific applications.¹² Quite often, the magnetic materials are studied for their use in the applications based on magnetic fields. But there are countless non-magnetic materials which are available with their own set of advantages and if their magnetic behavior is improved; their domain of applications can be greatly enhanced. The magnetic properties of certain materials can be enhanced by treating them with appropriate magnetic material by various means. Titanium dioxide NPs (TiO₂ NPs) belong to a class of metal oxide NPs which are gaining a lot of attention in the scientific community owing to their remarkable properties. Recently, they are being researched for their utilities in the medicine and healthcare industry. The concept of targeted drug delivery is the one for which researchers are rigorously studying these NPs for exploring the potential they possess. In order to obtain targeted drug delivery with the help of applied magnetic field, NPs bearing magnetic character are attached to pharmaceutical drugs and a setup of permanent magnetic arrays or superconducting magnets is utilized to ensure magnetically driven transport of the drug-loaded magnetic NPs.¹³ As far as TiO₂ NPs are concerned, they possess diamagnetic nature and sometimes exhibit very weak room temperature ferromagnetism.¹⁴ But their magnetic response can be relatively improved by doping or coating them with magnetic materials. Nowadays, the doping of TiO₂ NPs with magnetic materials, transition metals and rare-earth metals is receiving increasing interest from the researchers because of the introduction of magnetic behaviour into them. Mariano et al¹⁵ doped P25 TiO₂ NPs with different percentages of cobalt which exhibited anti-ferromagnetic behaviour at low temperatures and Curie-Weiss temperature increased with increasing dopant concentration. The dopant concentration and the synthesis process also affect the magnetic properties of the resulting samples. Raguram et al¹⁶ found that ferromagnetism was induced in Ni-doped and Cu-doped TiO₂ NPs, however, weak saturation magnetization values were obtained which can be improved by enhancing the dopant concentration or improvising the manufacturing process. Ravi et al¹⁷ observed room temperature ferromagnetism for TiO₂ NPs doped with molybdenum. Nithyaa et al¹⁸ reported that pure TiO₂ NPs display weak ferromagnetic behaviour whereas Nd-doped TiO₂ NPs exhibit unsaturated ferromagnetic behaviour at high field thereby proposing that unpaired electron pairs from rare earth metals interact with the host lattice and improve the magnetic interaction. In another study, they reported that the room temperature ferromagnetism of TiO₂ NPs was transformed into paramagnetic behaviour with the introduction of Gd ions as dopants into them.¹⁹ Zahid et al²⁰ doped the TiO₂ NPs with iron, the element is known to possess strong magnetic behaviour but found that the undoped sample exhibited the highest saturation magnetization

which decreased gradually with increasing dopant concentration. This striking observation was attributed to the larger crystallite size of the undoped TiO₂ NPs as saturation magnetization is strongly dependent on the crystallite size. The larger the crystallite size, the more is the saturation magnetization. Zhang et al²¹ conducted a study in which La ions were introduced into TiO₂ NPs without disturbing the tetragonal structure of the anatase phase. The addition of La ions modulates the concentration of oxygen vacancy in the sample which further modulates the room temperature magnetism in the NPs. Other than doping, the core-shell formulation is also opted for by the researchers in order to modify the magnetic properties of the NPs. The coating should offer good stability and furthermore, bioactive coatings are particularly favoured in medical applications.²² In this formulation, the NPs of the material to be modified either act as core or shell. Salamat et al²³ fabricated a magnetic core-shell Fe₃O₄@TiO₂ NPs and reported that the sample presented superparamagnetism but Fe₃O₄ alone presented a much higher degree of superparamagnetism. Furthermore, the saturation magnetization of Fe₃O₄ decreased due to the presence of the non-magnetic TiO₂ shell on the surface.

Thus, there is a lot of literature available regarding the usage of magnetic NPs or NPs doped with magnetic materials for targeted drug delivery systems. However, not much literature is available which discusses the changes, which take place in the host NPs after doping them with different materials, such as iron, rare-earth metals, and so on. One such example is TiO₂ NPs, which exhibit exceptional promise in drug-delivery applications and offer diamagnetic nature or weak ferromagnetic nature only for small values of magnetic fields. If an attempt is made to tailor their magnetic properties, then they can display remarkable magnetically controlled targeted drug delivery behaviour. Using this notion as the background of our current research, we have reported the synthesis of rutile TiO₂ NPs and then studied the changes occurring, if any, in their magnetic behaviour by doping/coating them with certain elements known to possess magnetic properties. The method used for synthesis affects the properties of the resulting NPs. Sharafabadi et al²⁴ observed that adopting an economical route of manufacturing via high energy ball milling followed by sintering resulted in nano-bioceramics with good compressive strength. In our study, we have opted for the sol-gel method, which is economical, easy and yields NPs of desired characteristics. Moreover, different chemicals are utilized for doping/coating purposes, although, in order to use nanomaterials for drug-delivery applications, their synthesis should be carried out with less toxic and biocompatible materials. Kazemi et al²⁵ synthesized bioactive nano-bioceramic using eggshell as raw material. The novelty of our work revolves around using Iron-supplement FericipXT for doping as well as for coating TiO₂ NPs. Thus, three samples were prepared of FericipXT-doped TiO₂ NPs with different dopant concentrations and three samples were prepared of FericipXT-coated TiO₂ NPs with different core:shell ratios. Next, Cerium (Ce), Erbium (Er) and Neodymium (Nd) were used for doping as the interaction of the ions present in rare earth metals are also known to maximize the magnetic behaviour of the host lattice. Depending upon the data received from Vibrating Sample Magnetometer (VSM), conclusions were drawn regarding the optimum way of improving the magnetic characteristics of rutile TiO₂ NPs.

Experimental Section

Materials

The materials used were Titanium Tetraisopropoxide (TTIP), ethanol, nitric acid (HNO₃), cerium nitrate, erbium nitrate, neodymium nitrate and deionized water (DI). They were obtained from Sigma Aldrich Pvt. Ltd., Bangalore, India, and were used as purchased without further refining. FericipXT tablets with folic acid by Cipla Ltd. were purchased from a chemist shop in Chandigarh. The basic safety control magnetic stirrer IKA-RCT IKAMAG with hot-plate by Merck, India, was used. A pH test kit from INSIF, India, was used to determine the final pH of the solution. A muffle furnace by INSIF, India, was used. Thomas Scientific's 30 mL high-aluminium conical crucibles were purchased for heating at higher temperatures.

Methods

Synthesis of Rutile TiO₂ NPs

The sol-gel method was used to synthesize TiO₂ NPs in the rutile phase. The calculated amount of Titanium Tetraisopropoxide (TTIP) was added to 50 mL of ethanol and stirred for half an hour. To this solution, 40 mL of DI water (deionized) and a controlled amount of nitric acid were added dropwise to achieve the desired pH of 1.0. The final

solution was stirred for one hour and then subjected to heating at 60°C. The initiation of heating resulted in the formation of a slurry. Thereafter, the obtained samples were further calcined at 800°C to obtain the TiO₂ NPs of desired phase and size.

Synthesis of FericipXT@TiO₂ Core-Shell NPs

To induce magnetic behaviour in rutile TiO₂ NPs so that they can be magnetically driven to the desired position, these NPs were modified with an iron coating, and thus FericipXT@TiO₂ NPs were synthesized. For this purpose, FericipXT tablets were used. Each film-coated tablet contains ferrous ascorbate equivalent to 100 mg elemental iron and 1.5 mg Folic Acid IP. For iron-coated TiO₂ NPs, the procedure mentioned by Mehr et. al²⁶ was followed. An optimal number of iron tablets were chosen for a core-to-shell ratio of 1:3, 1:1 and 3:1. Their intended amount was crushed and added to 250 mL of DI water. After the salt was completely dissolved, rutile TiO₂ NPs were mixed into the solution with continued stirring for 3 h. This was followed by dropwise addition of 1 M NaOH solution with continued stirring for 5 h. Finally, the solution was heated to reflux at 90°C. The resulting solution was centrifuged and washed with DI water to remove any impurities. The three different formulations of FericipXT-coated rutile TiO₂ NPs were further calcined at 800°C. The characteristic white colour of TiO₂ NPs was changed to light brown, brown and dark brown for 1:3, 1:1 and 3:1 core-shell formulations, respectively.

Synthesis of FericipXT-Doped TiO₂ NPs

FericipXT tablets were used for 1%, 3% and 5% doping in the TiO₂ NPs. A stoichiometric number of the tablets were dissolved in water for the respective percentage of the doping. Around 20 mL of the aqueous solution of the tablets were then added to the TTIP+ethanol solution formed by adding a stoichiometric quantity of TTIP in 40 mL ethanol followed by continuous stirring for an hour. Next, 7 mL of DI water mixed with nitric acid was added dropwise to the final solution by adjusting its pH. The solution was stirred for 1.5 hours and it was subjected to heating at 60°C for three hours. Post heating, the thick moist substance obtained was calcinated at 800°C for two hours. Finally, FericipXT-doped TiO₂ NPs were obtained. As the degree of doping was increased, the colour of the resulting NPs also displayed a stronger and stronger tinge of the dopant added.

Synthesis of Rare Earth Metals Doped TiO₂ NPs (Ce, Er and Nd)

Rare earth metals are also supposed to induce magnetic behaviour in the compounds. Thus, three rare-earth metals Ce, Er and Nd were doped in TiO₂ NPs with 5%, 10%, 15% and 20% composition by weight. Depending on the level of doping, a calculated amount of cerium nitrate/erbium nitrate/neodymium nitrate was dissolved in water. Around 20 mL of this solution was then added to the TTIP+ethanol solution formed by adding a stoichiometric quantity of TTIP in 40 mL ethanol followed by continuous stirring for an hour. Next, 7 mL of DI water mixed with nitric acid was added dropwise to the final solution by adjusting its pH. The solution was stirred for 1.5 hours and it was subjected to heating at 60°C for three hours. Post heating, the thick moist substance obtained was calcinated at 800°C for two hours. Finally, the rare-earth-doped TiO₂ NPs were obtained. As the degree of doping was increased, the colour of the resulting NPs also displayed a stronger and stronger tinge of the dopant added.

Characterization

The synthesized samples were characterized for X-ray Diffraction (XRD), High-Resolution Transmission Electron Microscopy (HR-TEM) and Vibrating Sample Magnetometer (VSM). XRD was carried out using Panalytical X'Pert Pro equipped with x'Celerator solid-state detector and manufactured by Panalytical, Netherlands. The sample was firmly placed onto the glass slide, which was carefully laid down onto the sample holder. XRD was performed at the Sophisticated Analytical Instrumentation Facility (SAIF), Panjab University, Chandigarh, India. HR-TEM was performed using Jeol 2100 Plus, Japan, at CIL, Panjab University, Chandigarh, India. A drop of the solution of powdered sample dispersed in ethanol was then carefully placed onto the copper grid. The grid was eventually air-dried under room temperature and was used for imaging after half an hour. Vibrating Sample Magnetometer (VSM) data was obtained through the Microsense EZ instrument. All the samples were characterized at room temperature. HighScore Plus software was used for the XRD analysis of the samples.

Results and Discussion

Figure 1A depicts the XRD plot of FericipXT-coated TiO₂ NPs in different ratios. FericipXT contains ferrous ascorbate salt along with folic acid, making it a major source of ferrous ions in our coating. Since the process of core-shell formation incorporates the mixing and heating of the iron tablets with TiO₂ NPs and the addition of a pH regulator, there is a possibility of the growth of several different iron-based oxides on the surface of the TiO₂ NPs. Tables 1, 2 and 3 present the compound name and crystal system of the relevant peaks obtained in the XRD plot for the 1:3, 1:1 and 3:1 core-shell formulation derived along with the corresponding JCPDS pattern. These observations have been obtained by analyzing the XRD plots via HighScore Plus software. The presence of different oxides of iron has ensured the presence of magnetic coating over the TiO₂ NPs. In our case of core-shell formulations, the ferrous ascorbate (C₁₂H₁₄FeO₁₂) present in the FericipXT tablet along with the TiO₂ core results in the formation of different iron-based and titanium-based oxides as gathered from the XRD data. In 1:3 core-shell formulation, different phases of TiO₂ were obtained because the concentration of the shell was kept 3 times lower than that of the core, indicating a greater diameter of the core (TiO₂) and a comparatively thinner shell. The resulting diffraction peaks either correspond to different titanium oxides or iron-titanium oxides.

In 1:1 core-shell formulation, different iron-based compounds were observed in the diffraction peaks and no phase of TiO₂ was observed while analyzing the XRD data. The presence of iron-based oxides ensures the modification of the magnetic behaviour of the resulting core-shell NPs. Similarly, in the 3:1 core-shell formulation, just 7% rutile phase of TiO₂ were observed, while the rest belonged to different oxides of iron. Rather et al²⁷ synthesized magnetic TiO₂ NPs by coating the surface of Fe₃O₄ NPs with TiO₂. The formation of Fe₃O₄ NPs was confirmed by the XRD plot as the diffraction peaks majorly corresponded to the magnetite (Fe₃O₄) phase. However, a few peaks corresponding to hematite and maghemite were also seen which could be attributed to the possible oxidation of magnetite. Similarly, in our observation, various iron-based oxides have been observed which have shown up due to the possible oxidation of FericipXT tablets.

Kermani et al²⁸ fabricated Fe₃O₄@SiO₂@TiO₂ magnetic core-shell NPs starting with Fe₃O₄ as the core NPs followed by a coating of SiO₂ and then a final coating with TiO₂. The XRD pattern depicted the diffraction peaks of both Fe₃O₄ and TiO₂ without any appreciable change in the individual diffraction peaks indicating an excellent crystallization taking place without disturbing the basic structure of Fe₃O₄ and TiO₂. Vlazan et al²⁹ developed TiO₂/ZnO core-shell NPs and both ZnO and TiO₂ peaks were visible in the diffraction data. Figure 1B displays the XRD plot for 1%, 3% and 5% FericipXT-doped TiO₂ NPs. The “*” mentioned in the plot for 5% doping refers to the low-intensity peaks of the maghemite phase. In 1% and 3% doped TiO₂ NPs, no stray peaks were visible other than the peaks of the pure rutile phase of TiO₂ NPs. Table 4 summarises the phases present and their % quantification in 1%, 3% and 5% FericipXT-doped TiO₂ NPs. The rutile TiO₂ NPs were obtained upon calcination at 800°C. The pH of the final solution was around 1.96. Fe-doped TiO₂ NPs developed by Barkhade et al³⁰ exhibited certain peaks belonging to the hematite phase of α-Fe₂O₃ for 0.5 and 1 mol. % Fe-doping.

Figure 1C illustrates the XRD plots for 5%, 10%, 15% and 20% cerium-doped TiO₂ NPs. The “*” indicated in the plots refers to cerium oxide (CeO_{1.6-2}TiO₂). Table 5 mentions the per cent quantification of different phases present in the samples so formed. From Table 5, it can be inferred that with an increase in % doping of cerium, the % quantification of cerium oxide in the resulting NPs also increased. Mikaeili et al³¹ developed Ce-doped TiO₂ NPs and reported that with the addition of Ce atom, the rutile phase content in the resulting sample increased. In our case, for 5% doping almost comparable anatase and rutile phases were obtained. However, when % doping was increased to 10% and then to 15%, the percentage of anatase content increased, while that of the rutile content decreased. In other words, when the % doping was increased from 5% to 15%, the % quantification of anatase phase increased and that of the rutile phase decreased. But, at 20% doping, a reversal of phase dominance was observed and approximately 72% rutile phase and 15% anatase phase content was obtained in the resulting NPs. Thus, it can be concluded that the % doping of cerium as high as 20% favours the growth of rutile phase.

Figure 1D illustrates the XRD plots for 5%, 10%, 15% and 20% erbium-doped TiO₂ NPs. For 5% and 20% doping, only anatase phase of TiO₂ NPs was obtained, whereas in 10% doping, rutile was the only phase and for 15% doping, both anatase and rutile phases were present. From 5% to 15% doping, erbium titanium oxide peaks were obtained in the

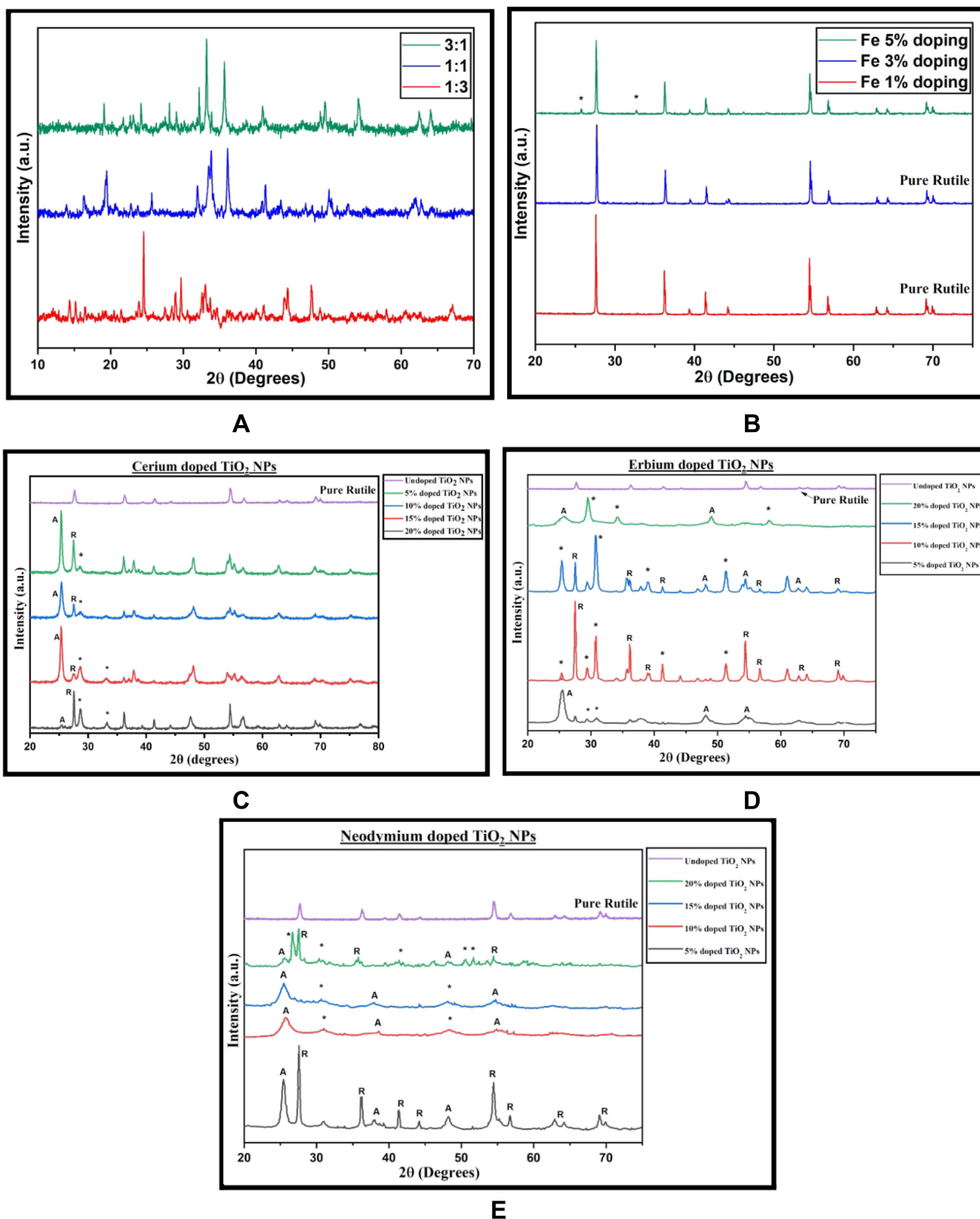


Figure 1 XRD plot of (A) core-shell FericipXT@TiO₂ NPs in 1:3, 1:1 and 3:1 ratios, (B) 1%, 3% and 5% FericipXT-doped TiO₂ NPs (the “*” mentioned in the plot for 5% doping refers to the low-intensity peaks of the maghemite phase), (C) 5%, 10%, 15% and 20% Ce-doped TiO₂ NPs (the “*” indicated in the plots refers to cerium oxide (CeO_{1.6}2TiO₂)), (D) 5%, 10%, 15% and 20% Er-doped TiO₂ NPs (the “*” mentioned in the plot corresponds to the erbium titanium oxide and erbium oxide phases so obtained) and (E) 5%, 10%, 15% and 20% Nd-doped TiO₂ NPs (the “*” corresponds to neodymium titanium oxide).

Table 1 The Description of Different Peaks Which Were Obtained in the XRD Plot for 1:3 FericipXT@TiO₂ Core-Shell NPs

| 1:3 | | |
|---------------|--|----------------|
| JCPDS Pattern | Compound Name | Crystal System |
| 01-085-1410 | Iron - alpha (Fe) | Cubic |
| 01-076-0145 | Titanium (III) oxide (Ti ₂ O ₃) | Rhombohedral |
| 01-073-1765 | Rutile Titanium dioxide (TiO ₂) | Tetragonal |
| 00-033-1381 | Titanium oxide (TiO ₂) | Hexagonal |
| 01-073-1256 | (Ilmenite) Iron Titanium oxide (Fe _{1.10} Ti _{0.90} O ₃) | Rhombohedral |
| 00-046-1237 | Titanium oxide (TiO ₂) | Monoclinic |
| 01-072-2325 | (Landauite) Titanium iron oxide (Ti ₂ Fe ₂ O ₇) | Monoclinic |
| 01-075-1211 | (Ilmenite) Iron Titanium Oxide (FeTiO ₃) | Rhombohedral |
| 01-085-1059 | Titanium oxide (Ti ₇ O ₁₃) | Anorthic |

Table 2 The Description of Different Peaks Which Were Obtained in the XRD Plot for 1:1 FericipXT@TiO₂ Core-Shell NPs

| 1:1 | | | |
|---------------|---|----------------|----------------|
| JCPDS Pattern | Compound Name | Quantification | Crystal System |
| 01-084-0311 | Iron (III) oxide- alpha (Fe ₂ O ₃) | 8.9% | Rhombohedral |
| 01-089-2428 | Dioxygen-alpha (O ₂) | 17.8% | Monoclinic |
| 01-089-0599 | (Hematite) Iron (III) oxide-alpha (Fe ₂ O ₃) | 5% | Rhombohedral |
| 01-076-1821 | Iron (III) oxide-beta (Fe ₂ O ₃) | 24.8% | Hexagonal |
| 01-086-1350 | Iron Oxide (Fe _{2.937} O ₄) | 1% | Cubic |
| 01-080-2186 | Iron oxide-gamma (Fe _{21.34} O ₃₂) | 19.8% | Tetragonal |
| 01-089-5894 | (Maghemite Q Iron Oxide) Iron (III) oxide-gamma (Fe _{1.966} O _{2.963}) | 22.7% | Tetragonal |

plots but for 20% doping, a proper erbium oxide phase was obtained. The “*” mentioned in the plot corresponds to phases of different erbium-based oxides so obtained. Clearly, the erbium concentration in the samples increased with the increased % doping. Table 6 highlights the phases and their % quantification in the Er-doped samples obtained. 5% doped NPs showed a characteristic anatase peak at 25.4°. But the rest of the plot exhibited lesser crystallinity. The crystallinity elevated in 10% and 15% doped NPs which again dropped down in 20% doped NPs. The peaks were having decreased intensity with visible broadening. Venkatachalam et al³² observed a strain occurring in the system along with peak broadening and reduction in crystallite size when TiO₂ NPs were doped with Er³⁺ ions. Talane et al³³ observed a decrease in the intensity of the diffraction peaks with increasing concentration of Er³⁺ ions as dopants in TiO₂ NPs indicating a decrease in the crystallinity of the doped samples.

Figure 1E illustrates the XRD plots for 5%, 10%, 15% and 20% neodymium-doped TiO₂ NPs. The TiO₂ NPs having 5% Nd-doping displayed a mixed anatase-rutile phase with zero neodymium content. With an increase in doping concentration from 10% to 20%, the content of neodymium titanium oxide showed an increasing trend. The presence of neodymium titanium oxide

Table 3 The Description of Different Peaks Which Were Obtained in the XRD Plot for 3:1 FericipXT@TiO₂ Core-Shell NPs

| 3:1 | | | |
|---------------|---|----------------|----------------|
| JCPDS Pattern | Compound Name | Quantification | Crystal System |
| 01-079-1741 | (Hematite) Iron oxide-alpha (Fe ₂ O ₃) | 28% | Rhombohedral |
| 01-089-2776 | Dioxygen-beta (O ₂) | 9% | Rhombohedral |
| 01-082-0514 | Rutile Titanium dioxide (TiO ₂) | 7% | Tetragonal |
| 01-075-1212 | (Ilmenite) Iron Titanate (FeTiO ₃) | 10% | Rhombohedral |
| 01-083-0112 | Maghemite C subcell Iron Oxide (Fe _{21.333} O ₃₂) | 18% | Cubic |
| 01-089-5894 | (Maghemite Q Iron Oxide) Iron (III) oxide-gamma (Fe _{1.966} O _{2.963}) | 28% | Tetragonal |

Table 4 The Description of Different Phases Which Were Obtained in the XRD Plot for Different Percentages of FericipXT-Doped TiO₂ NPs

| Iron Doping | |
|-------------|---|
| % Doping | Phases and Their Quantification |
| 1% | 100% Rutile (01-088-1172), (01-078-1510) |
| 3% | 100% Rutile (01-088-1172), (01-078-1510), (01-078-1508) |
| 5% | 65% Monoclinic (TiO ₂) (01-082-1137) 29% Rutile (01-088-1172), (01-089-4920) 5% Iron Titanium Oxide (01-073-1631) 1% Anatase (01-075-1537) |

Table 5 The Description of Different Phases Which Were Obtained in the XRD Plot for Different Percentages of Cerium-Doped TiO₂ NPs

| Cerium Doping | |
|---------------|---|
| % Doping | Phases and Their Quantification |
| 5% | 51.5% Anatase (01-084-1286) 46.5% Rutile (01-089-0554) 2% Cerium Oxide (CeO _{1.6} .2TiO ₂) (03-065-5923) |
| 10% | 65% Anatase (01-086-1156) 32% Rutile (01-089-4920) 3% Cerium Oxide (03-065-5923) |
| 15% | 79% Anatase (01-086-1156) 15% Rutile (03-065-0191) 6% Cerium Oxide (03-065-5923) |
| 20% | 72% Anatase (01-086-1155) 15% Rutile (01-084-1284) 13% Cerium Oxide (03-065-5923) |

Table 6 The Description of Different Phases Which Were Obtained in the XRD Plot for Different Percentages of Erbium-Doped TiO₂ NPs

| Erbium Doping | |
|---------------|--|
| % Doping | Phases and Their Quantification |
| 5% | 96% Anatase (01-089-4921) 4% Erbium Titanium Oxide (01-073-1700) |
| 10% | 90% Rutile (01-089-4920) 10% Erbium Titanium Oxide (01-073-1647) |
| 15% | 37% Anatase (01-086-1156) 43% Rutile (01-089-4920) 20% Erbium Titanium Oxide (01-073-1700) |
| 20% | 63% Anatase (01-075-1537) 37% Erbium Oxide (01-074-1983) |

can be attributed to the addition of a greater percentage of Nd concentration. Rutile phase was detected in 5% doped and 20% doped-TiO₂ NPs while it was absent in the 10% doped and 15% doped-TiO₂ NPs. The anatase phase showed a decreasing trend from 10% doping onwards. The crystallinity of the resulting sample for 20% doping also declined. Table 7 showcases the phases, their per cent quantifications and the corresponding JCPDS patterns of the different Nd-doped TiO₂ NPs. The “*” depicted in the corresponding XRD plot relates to neodymium titanium oxide. Liang et al³⁴ synthesized the Nd-doped TiO₂ NPs and observed that the addition of Nd ions favoured the anatase phase. The pristine TiO₂ NPs exhibited a mixed anatase-rutile phase with a dominant characteristic rutile peak, but the rutile phase was completely absent in the Nd-doped TiO₂ NPs.

In our study, the crystallite size calculated from the Debye-Scherrer equation for FericipXT-doped TiO₂ NPs showed a decline with an increase in % doping as mentioned in Table 8. The crystallite size decreased slightly with increasing dopant concentration. Khan et al³⁵ reported a reduction in the crystallite size of the TiO₂ NPs on doping with iron. Table 9 describes the crystallite sizes obtained for different percent doping of Ce, Er and Nd in TiO₂ NPs. In case of cerium-doping, for 5% and 10% doping, ~23 nm crystallite size was obtained which dropped down to 17.68 nm for 15% doping and then shot to 29.83 nm for 20% doping. Menezes et al³⁶ fabricated Ce-doped TiO₂ NPs and observed that at 5 mol% doping, low-intensity ceria peaks originated which became more prominent for 10 mol% doping. In addition to

Table 7 The Description of Different Phases Which Were Obtained in the XRD Plot for Different Percentages of Neodymium-Doped TiO₂ NPs

| Neodymium Doping | |
|------------------|--|
| % Doping | Phases and Their Quantification |
| 5% | 45% Anatase (01-073-1764) 55% Rutile (01-078-1510) |
| 10% | 62% Anatase (01-083-2243) 38% Neodymium Titanium Oxide (01-081-0950) |
| 15% | 27% Anatase (01-083-2243) 73% Neodymium Titanium Oxide (01-081-0270) |
| 20% | 8% Anatase (01-075-1537) 16% Rutile (01-089-4920) 76% Neodymium Titanium Oxide (00-032-0684), (00-039-1118), (01-081-0270) |

Table 8 The Crystallite Sizes of Iron Doped-TiO₂ NPs Obtained for Different Percentages Doping

| Dopant → Concentration ↓ | Iron |
|-----------------------------|----------|
| 1% | 79.66 nm |
| 3% | 66.83 nm |
| 5% | 63.27 nm |

Table 9 The Crystallite Sizes of Doped-TiO₂ NPs Obtained for Different Percentage Doping of Rare-Earth Metals

| Dopant → Concentration ↓ | Cerium | Erbium | Neodymium |
|-----------------------------|----------|----------|-----------|
| 5% | 22.73 nm | 22.85 nm | 27.16 nm |
| 10% | 23.46 nm | 33.48 nm | 14.34 nm |
| 15% | 17.68 nm | 28.07 nm | 12.21 nm |
| 20% | 29.83 nm | 16.28 nm | 23.94 nm |

this, the relationship between % ceria doping and the crystallite size was found to be non-linear. The broadening in peak is associated with a reduction in grain size, and this is validated from the least crystallite size obtained for the 20% erbium-doped TiO₂ NPs compared to the rest of the three samples. Furthermore, no particular trend of change in the crystallite size was detected with the increase in % doping, rather a non-linear behaviour was observed as shown in Table 9. The change in crystallite size with an increase in % doping of neodymium showed an abnormal trend. The crystallite sizes obtained for 5% and 10% doping were comparable, and those obtained for 15% and 20% doping were relatable. Nithyaa et al³⁷ observed a decline in the mass fraction of the anatase phase of the doped TiO₂ NPs with an increasing concentration of Nd ions. Additionally, a decreasing trend in crystallite size of the doped NPs was obtained with increasing Nd concentration. One peculiar observation made here is that the crystallite sizes obtained for FericipXT-doped TiO₂ NPs were much greater than those obtained for Ce, Er and Nd-doped TiO₂ NPs, although, the synthesis process was similar for all and all the samples were calcined at 800°C. For FericipXT-doped TiO₂ NPs, highly crystalline narrow diffraction peaks were obtained which led to greater crystallite size.

The size and morphology of the synthesized samples were recorded using HRTEM. Furthermore, ImageJ software was used to analyze the HR-TEM micrographs of the core-shell NPs. The HR-TEM images depict the size of ~30–50 nm for 1:3, ~70 nm for 1:1 and ~95 nm for 3:1, respectively. In Figure 2A, the darker portion corresponds to TiO₂ and the lighter portion across it displays the coating. Since the core-shell formulation was 1:3, the concentration of the core was greater than that of the shell. Thus, we can see a faint coating over the nanoparticle. Figure 2B presents the 1:1 core-shell formulation. Both the inner and the outer layers look alike in proportion. Figure 2C illustrates the 3:1 core-shell formulation and as a result, a very tiny core with quite a thick outer coating can be seen. Moreover, all three core-shell formulations exhibited a nearly spherical shape.

The VSM study was conducted on the synthesized samples to understand the magnetic behaviour displayed by them. Figure 3A shows the VSM plot for FericipXT-coated rutile TiO₂ NPs with different core-shell ratios. We can clearly infer that the magnetization displayed by the sample increased with the increase in the iron content of the shell. The inset in Figure 3A depicts the VSM plot for 1:3 core-shell TiO₂ NPs as the exact shape of the curve was not visible when plotted along with the data of 1:1 and 3:1 core-shell TiO₂ NPs. Both 1:3 and 1:1 core-shell NPs exhibited superparamagnetic behaviour; however, a narrower loop was obtained for 3:1 core-shell NPs which is indicative of their ferromagnetic nature. Xu et al³⁸ combined

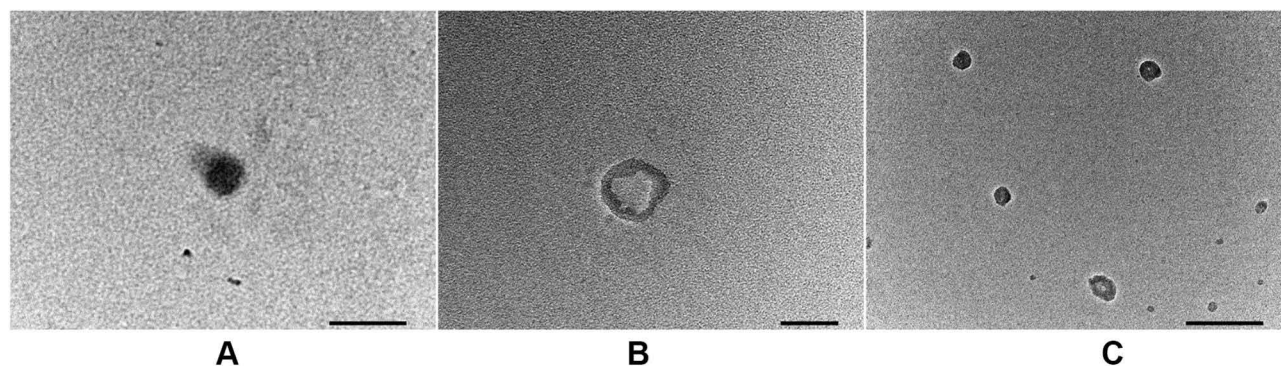


Figure 2 HR-TEM image of FericipXT-coated TiO₂ NPs with core-shell ratio of (A) 1:3, (B) 1:1 and (C) 3:1.

Fe₃O₄ core with La-based MOF (Metal-Organic Framework) shell in order to have meticulous dual-mode imaging and then used them for loading and transport of Doxorubicin. **Figure 3B** depicts the VSM plots obtained for 1%, 3% and 5% FericipXT-doped rutile TiO₂ NPs. The 3% doped sample showed paramagnetic behaviour with a very weak ferromagnetic contribution at lower magnetic fields. Both 1% and 5% doped samples showed narrow hysteresis loops, indicating their ferromagnetic character with the retentivity of the 5% doped sample more than the 1% doped sample. With this study, we have observed that the magnetization induced in the doped samples is much less than that induced in the core-shell NPs. Cynthia et al³⁹ developed Fe-doped TiO₂ NPs and room temperature ferromagnetism was observed. Tolea et al⁴⁰ reported in their study that the weak room temperature ferromagnetism observed in Fe-doped TiO₂ NPs is not dependent on Fe-doping as the Fe ions are not ferromagnetic at room temperature. An increase in the iron content increases the oxygen vacancies in the sample thereby enhancing the ferromagnetic saturation magnetization. Any type of thermal treatment strongly reduces the Fe³⁺ ions and converts them into Fe²⁺ ions. TiO₂ NPs were doped with rare-earth metals (Ce, Er, Nd) to study the difference occurring in their magnetic behaviour after rare-earth doping. Nithyaa et al¹⁹ observed a magnetic transition from ferromagnetic phase to paramagnetic phase in Gd-doped TiO₂ NPs with increasing Gd-content. **Figure 3C and 3D** depict the VSM plots of Ce-doped TiO₂ NPs and a room temperature ferromagnetic behaviour can be seen in all the samples. The magnetization induced in 5%, 10% and 20% Ce-doped NPs was lesser than that induced in 15% Ce-doped TiO₂ NPs due to which the VSM plot of 15% Ce-doped TiO₂ NPs has been shown separately in **Figure 3D**. Undoped TiO₂ NPs also demonstrated weak ferromagnetism with 0.004 emu/g saturation magnetization, which further declined in the case of 5% and 20% Ce-doped TiO₂ NPs. However, for 10% doping, the value of saturation magnetization rose to 0.007 emu/g. Furthermore, 15% Ce-doped TiO₂ NPs possess a saturation magnetization of 1.5 emu/g which is much greater than the other three samples. **Figure 3E** illustrates the VSM plots for Erbium-doped TiO₂ NPs. Typical staircase-like plots have been obtained for 5%, 10%, 15% and 20% Er-doped TiO₂ NPs. It can be observed that with the increase in the dopant concentration, the plots have gone considerably steeper.

In the case of Er-doped TiO₂ NPs, 5% of doped NPs have stretched out staircase-like structure, which keeps on shrinking further and further with the increase in per cent doping. In 20% Er-doped TiO₂ NPs, the staircase-like plot expands only between -10,000 Oe to +10,000 Oe and beyond that the plot shows a straight line which is characteristic of paramagnetic behaviour. **Figure 3F** shows the VSM plots obtained for Nd-doped TiO₂ NPs. Again, larger staircase-like plots have been obtained with an exception for 5% Nd-doped TiO₂ NPs which depicts a straight line with a negative slope indicating the diamagnetic nature of the synthesized sample. No typical hysteresis loops were observed for Er-doped and Nd-doped TiO₂ NPs. Among all the samples synthesized, the magnetization attained in the treated TiO₂ NPs is maximum in core-shell NPs.

Thus, coating the NPs with magnetic material offers a better option for modifying the magnetic behaviour of the otherwise non-magnetic NPs. These magnetic-responsive NPs are potential candidates for magnetically driven drug delivery inside the human body. Further research needs to be undertaken to improve the magnetic sensitivity of the NPs so that they can be effectively utilized for a plethora of applications. Now, we know that non-magnetic NPs can also be modified to deliver magnetic behaviour via different treatments such as doping or coating.

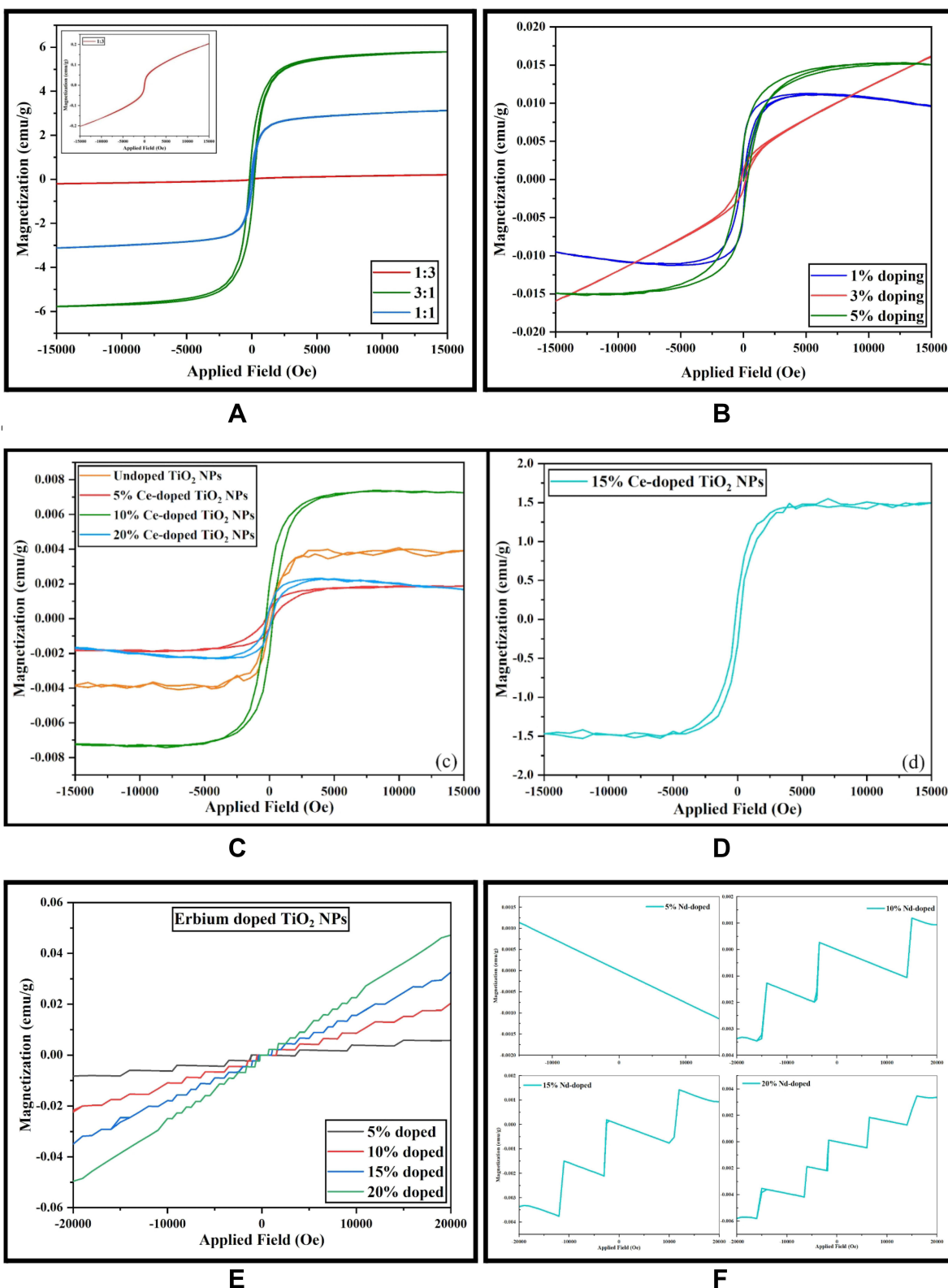


Figure 3 VSM plots of (A) 1:3, 1:1 and 3:1 FerriPXT@TiO₂ core-shell NPs, (B) 1%, 3% and 5% FerriPXT-doped TiO₂ NPs, (C) 5%, 10% and 20% Ce-doped TiO₂ NPs, (D) 15% Ce-doped TiO₂ NPs, (E) 5%, 10%, 15% and 20% Er-doped TiO₂ NPs and (F) 5%, 10%, 15% and 20% Nd-doped TiO₂ NPs.

Conclusion

The magnetic properties of TiO₂ NPs were optimized by coating or doping them with magnetic materials such as FericipXT (iron supplement) and rare-earth metals (Ce, Er and Nd). Iron supplement-doped TiO₂ NPs belonged to the rutile phase for 1% and 3% doping, but extra peaks corresponding to the maghemite phase emerged for 5% doping. XRD patterns of Ce-doped, Er-doped and Nd-doped TiO₂ NPs possessed phases of TiO₂ NPs (anatase/rutile/mixed) along with the oxide phases of the corresponding rare-earth metal. It was observed that doping of 5% and higher resulted in extra phases in the resulting NPs originating due to the dopant added. The XRD plots of core-shell NPs depicted the presence of various iron titanium oxides and iron oxides. The coating of FericipXT over TiO₂ NPs at different ratios suggested that FericipXT was loaded in amorphous form and thus, the resulting NPs had lesser crystallinity than the original rutile TiO₂ NPs. The successful formation of 1:3, 1:1 and 3:1 core-shell TiO₂ NPs was confirmed from the HR-TEM images. FericipXT-doped and Ce-doped TiO₂ NPs exhibited ferromagnetism. Er-doped and Nd-doped TiO₂ NPs displayed a slightly peculiar step-like hysteresis plot. Among all the samples, FericipXT-coated TiO₂ NPs demonstrated maximum saturation magnetization with superparamagnetic behaviour turning into ferromagnetic with increasing concentration of the shell material. It was deduced that coating with a magnetic material drastically improves the magnetic character of the host NPs. Thus, the magnetic properties of the TiO₂ NPs can be tweaked by treating them with suitable materials. Efforts should be made to enhance the magnetic features even more so that these NPs can be successfully utilized for magnetically guided drug delivery and magnetic hyperthermia applications.

Acknowledgment

We are grateful to the Sophisticated Analytical Instrumentation Facility (SAIF) and CIL, Panjab University, Chandigarh, for timely characterizations. We are grateful to Dr. Sanjeev Gautam, Assistant Professor, UICET, Panjab University, Chandigarh for providing us with access to HighScore Plus software.

Funding

This research has not received any specific grants from funding agencies in the public, commercial or non-profit sectors.

Disclosure

The authors report no conflicts of interest in this work.

References

1. Bagheri S, Hashemian M, Khosravi M, Khandan A. An experimental investigation of novel hybrid epoxy/glass fibers nanocomposite reinforced with nanoclay with enhanced properties for low velocity impact test. *J Nanostruct.* 2020;10(1):92–106. doi:10.22052/JNS.2020.01.011
2. Takmil F, Esmaili H, Mousavi SM, Hashemi SA. Nano-magnetically modified activated carbon prepared by oak shell for treatment of wastewater containing fluoride ion. *Adv Powder Technol.* 2020;31(8):3236–3245. doi:10.1016/j.appt.2020.06.015
3. Mousavi M, Hashemi A, Arjmand O, et al. Erythrosine adsorption from aqueous solution via decorated graphene oxide with magnetic iron oxide nano particles: kinetic and equilibrium studies. *Acta Chim Slov.* 2018;65(4):882–894. doi:10.17344/acsi.2018.4537
4. Mousavi SM, Hashemi SA, Amani AM, et al. Pb (II) removal from synthetic wastewater using Kombucha Scoby and graphene oxide/Fe₃O₄. *Phys Chem Res.* 2018;6(4):759–771. doi:10.22036/PCR.2018.133392.1490
5. Parvin N, Babapoor A, Nematollahzadeh A, Mousavi SM. Removal of phenol and β-naphthol from aqueous solution by decorated graphene oxide with magnetic iron for modified polyrhodanine as nanocomposite adsorbents: kinetic, equilibrium and thermodynamic studies. *React Funct Polym.* 2020;156:104718. doi:10.1016/j.reactfunctpolym.2020.104718
6. Hashemi SA, Mousavi SM, Bahrani S, Ramakrishna S, Hashemi SH. Picomolar-level detection of mercury within non-biological/biological aqueous media using ultra-sensitive polyaniline-Fe₃O₄-silver diethyldithiocarbamate nanostructure. *Anal Bioanal Chem.* 2020;412(22):5353–5365. doi:10.1007/s00216-020-02750-1
7. Gholami A, Mousavi SM, Hashemi SA, Ghasemi Y, Chiang WH, Parvin N. Current trends in chemical modifications of magnetic nanoparticles for targeted drug delivery in cancer chemotherapy. *Drug Metab Rev.* 2020;52(1):205–224. doi:10.1080/03602532.2020.1726943
8. Soltani M, Tehrani MHH, Kashkooli FM, Rezaeian M. Effects of magnetic nanoparticle diffusion on microwave ablation treatment: a numerical approach. *J Magn Magn Mater.* 2020;514:167196. doi:10.1016/j.jmmm.2020.167196
9. Salmani MM, Hashemian M, Khandan A. Therapeutic effect of magnetic nanoparticles on calcium silicate bioceramic in alternating field for biomedical application. *Ceram Int.* 2020;46(17):27299–27307. doi:10.1016/j.ceramint.2020.07.215
10. Mousavi SM, Hashemi SA, Gholami A, et al. Bioinorganic synthesis of polyrhodanine stabilized Fe₃O₄/Graphene oxide in microbial supernatant media for anticancer and antibacterial applications. *Bioinorg Chem Appl.* 2021;2021:1–12. doi:10.1155/2021/9972664
11. Rezaeian M, Soltani M, Karimvand AN, Raahemifar K. Mathematical modeling of targeted drug delivery using magnetic nanoparticles during intraperitoneal chemotherapy. *Pharmaceutics.* 2022;14(2):324. doi:10.3390/pharmaceutics14020324

12. Najafinezhad A, Abdellahi M, Ghayour H, Soheily A, Chami A, Khandan A. A comparative study on the synthesis mechanism, bioactivity and mechanical properties of three silicate bioceramics. *Mater Sci Eng C*. 2017;72:259–267. doi:10.1016/j.msec.2016.11.084
13. Zahn D, Klein K, Radon P, et al. Investigation of magnetically driven passage of magnetic nanoparticles through eye tissues for magnetic drug targeting. *Nanotechnology*. 2020;31(49):495101. doi:10.1088/1361-6528/abb0b4
14. Bhullar S, Goyal N, Gupta S. Rapid green-synthesis of TiO₂ nanoparticles for therapeutic applications. *RSC Adv*. 2021;11(48):30343–30352. doi:10.1039/D1RA05588G
15. Mariano JFML, Bessergenev VG, Lourenço JP, et al. Structural and magnetic properties of P25 TiO₂ nanoparticles doped by Co. *J Magn Magn Mater*. 2020;501:166442. doi:10.1016/j.jmmm.2020.166442
16. Raguram T, Rajni KS. Synthesis and analysing the structural, optical, morphological, photocatalytic and magnetic properties of TiO₂ and doped (Ni and Cu) TiO₂ nanoparticles by sol–gel technique. *Appl Phys A*. 2019;125:288. doi:10.1007/s00339-019-2581-1
17. Ravi S, Shashikanth FW. Magnetic properties of Mo-doped TiO₂ nanoparticles: a candidate for dilute magnetic semiconductors. *Mater Lett*. 2020;264:127331. doi:10.1016/j.matlet.2020.127331
18. Nithyaa N, Jaya NV. Effect of Nd on structural, optical and magnetic behaviour of TiO₂ nanoparticles. *Appl Phys A*. 2021;127:69. doi:10.1007/s00339-020-04140-x
19. Nithyaa N, Jaya NV. Structural, optical, and magnetic properties of Gd-doped TiO₂ nanoparticles. *J Supercond Nov Magn*. 2018;31:4117–4126. doi:10.1007/s10948-018-4693-9
20. Zahid R, Manzoor M, Rafiq A, et al. Influence of iron doping on structural, optical and magnetic properties of TiO₂ nanoparticles. *Electron Mater Lett*. 2018;14:587–593. doi:10.1007/s13391-018-0060-z
21. Zhang H, Wang Y, Zhong W, Long B, Wu Y, Xie Z. Tailoring the room temperature ferromagnetism in TiO₂ nanoparticles by modulating the concentration of surface oxygen vacancy via La incorporating. *Ceram Int*. 2019;45(10):12949–12956. doi:10.1016/j.ceramint.2019.03.222
22. Khandan A, Abdellahi M, Ozada N, Ghayour H. Study of the bioactivity, wettability and hardness behaviour of the bovine hydroxyapatite-diopside bio-nanocomposite coating. *J Taiwan Inst Chem Eng*. 2016;60:538–546. doi:10.1016/j.jtice.2015.10.004
23. Salamat S, Younesi H, Bahramifar N. Synthesis of magnetic core–shell Fe₃O₄@TiO₂ nanoparticles from electric arc furnace dust for photocatalytic degradation of steel mill wastewater. *RSC Adv*. 2017;7(31):19391–19405. doi:10.1039/C7RA01238A
24. Sharafabadi AK, Abdellahi M, Kazemi A, Khandan A, Ozada N. A novel and economical route for synthesizing akermanite (Ca₂MgSi₂O₇) nano-bioceramic. *Mater Sci Eng C*. 2017;71:1072–1078. doi:10.1016/j.msec.2016.11.021
25. Kazemi A, Abdellahi M, Khajeh-Sharafabadi A, Khandan A, Ozada N. Study of in vitro bioactivity and mechanical properties of diopside nano-bioceramic synthesized by a facile method using eggshell as raw material. *Mater Sci Eng C*. 2017;71:604–610. doi:10.1016/j.msec.2016.10.044
26. Mehr ME, Maleki-Ghaleh H, Yarahmadi M, Kavanlouei M, Siadati MH. Synthesis and characterization of photocatalytic zinc oxide/titanium oxide (core/shell) nanocomposites. *J Alloys Compd*. 2021;882:160777. doi:10.1016/j.jallcom.2021.160777
27. Rather M, Bhaskarwar A, Fabrication of magnetic TiO₂ nanoparticles for use in photocatalytic process, Proceedings of the International Conference on Advances in Chemical Engineering, NITK Surathkal, India, 2015, Paper No. 165.
28. Kermani M, Kakavandi B, Farzadkia M, Esrafil A, Jokandan SF, Shahsavani A. Catalytic ozonation of high concentrations of catechol over TiO₂@Fe₃O₄ magnetic core-shell nanocatalyst: optimization, toxicity and degradation pathway studies. *J Clean Prod*. 2018;192:597–607. doi:10.1016/j.jclepro.2018.04.274
29. Vlazan P, Ursu DH, Irina-Moiescu C, Miron I, Sfirloaga P, Rusu E. Structural and electrical properties of TiO₂/ZnO core–shell nanoparticles synthesized by hydrothermal method. *Mater Charact*. 2015;101:153–158. doi:10.1016/j.matchar.2015.01.017
30. Barkhade T, Mishra S, Chander H, Mahapatra SK, Banerjee I. Effect of TiO₂ and Fe doped TiO₂ nanoparticles on mitochondrial membrane potential in HBL-100 cells. *Biointerphases*. 2019;14(4):041003. doi:10.1116/1.5097643
31. Mikaeili F, Topcu S, Jodhani G, Gouma P-I. Flame-sprayed pure and Ce-doped TiO₂ photocatalysts. *Catalysts*. 2018;8:342. doi:10.3390/catal8090342
32. Venkatachalam P, Kalaivani T, Krishnakumar N. Erbium doped anatase TiO₂ nanoparticles for photovoltaic applications. *Opt Quant Electron*. 2019;51:315. doi:10.1007/s11082-019-2034-2
33. Talane TE, Mbule PS, Noto LL, et al. Sol-gel preparation and characterization of Er³⁺ doped TiO₂ luminescent nanoparticles. *Mater Res Bull*. 2018;108:234–241. doi:10.1016/j.materresbull.2018.09.007
34. Liang J, Wang J, Song K, Wang X, Yu K, Liang C. Enhanced photocatalytic activities of Nd-doped TiO₂ under visible light using a facile sol-gel method. *J Rare Earths*. 2020;38(2):148–156. doi:10.1016/j.jre.2019.07.008
35. Khan MS, Shah JA, Riaz N, et al. Synthesis and characterization of Fe-TiO₂ nanomaterial: performance evaluation for RB5 decolorization and in vitro antibacterial studies. *Nanomaterials*. 2021;11:436. doi:10.3390/nano11020436
36. Menezes BAT, Moreira DEB, Oliveira HA, Marquesa LF, Lima JF. Solvothermal synthesis of cerium-doped titania nanostructured materials modified with acetylacetone for solar-driven photocatalysis. *J Braz Chem Soc*. 2020;31(1):153–161. doi:10.21577/0103-5053.20190148
37. Nithyaa N, Bhoopathi G, Magesha G, Kumar CDN. Neodymium doped TiO₂ nanoparticles by sol-gel method for antibacterial and photocatalytic activity. *Mater Sci Semicond Process*. 2018;83:70–82. doi:10.1016/j.mssp.2018.04.011
38. Xu C, Zhang C, Wang Y, Li L, Li L, Whittaker AK. Controllable synthesis of a novel magnetic core–shell nanoparticle for dual-modal imaging and pH-responsive drug delivery. *Nanotechnology*. 2017;28(49):495101. doi:10.1088/1361-6528/aa929b
39. Cynthia S, Sagadevan S. Physicochemical and magnetic properties of pure and Fe doped TiO₂ nanoparticles synthesized by sol-gel method. *Mater Today: Proc*. 2022;50(7):2720–2724.
40. Tolea F, Grecu MN, Kuncser V, Constantinescu SG, Ghica D. On the role of Fe ions on magnetic properties of doped TiO₂ nanoparticles. *Appl Phys Lett*. 2015;106(14):142404. doi:10.1063/1.4917037

International Journal of Nanomedicine

Dovepress

Publish your work in this journal

The International Journal of Nanomedicine is an international, peer-reviewed journal focusing on the application of nanotechnology in diagnostics, therapeutics, and drug delivery systems throughout the biomedical field. This journal is indexed on PubMed Central, MedLine, CAS, SciSearch[®], Current Contents[®]/Clinical Medicine, Journal Citation Reports/Science Edition, EMBase, Scopus and the Elsevier Bibliographic databases. The manuscript management system is completely online and includes a very quick and fair peer-review system, which is all easy to use. Visit <http://www.dovepress.com/testimonials.php> to read real quotes from published authors.

Submit your manuscript here: <https://www.dovepress.com/international-journal-of-nanomedicine-journal>